Analysis of the resistive switching behaviors of vanadium oxide thin film*

Wei Xiao-Ying(韦晓莹)[a], Hu Ming(胡 明)[a], Zhang Kai-Liang(张楷亮)[b]†, Wang Fang(王 芳)[b], Zhao Jin-Shi(赵金石)[b], and Miao Yin-Ping(苗银萍)[b]

[a] School of Electronics Information Engineering, Tianjin University, Tianjin 300072, China

[b] School of Electronics Information Engineering, Tianjin Key Laboratory of Film Electronic & Communication Devices, Tianjin University of Technology, Tianjin 300384, China

(Received 7 July 2012; revised manuscript received 21 August 2012)

We demonstrate the polarization of resistive switching for a Cu/VO_x/Cu memory cell. The switching behaviors of Cu/VO_x/Cu cell are tested by using a semiconductor device analyzer (Agilent B1500A), and the relative micro-analysis of *I–V* characteristics of VO_x/Cu is characterized by using a conductive atomic force microscope (CAFM). The *I–V* test results indicate that both the forming and the reversible resistive switching between low resistance state (LRS) and high resistance state (HRS) can be observed under either positive or negative sweep. The CAFM images for LRS and HRS directly exhibit evidence for the formation and rupture of filaments based on positive or negative voltage. The Cu/VO_x/Cu sandwiched structure exhibits reversible resistive switching behavior and shows potential applications in the next generation of nonvolatile memory.

Keywords: VO_x thin films, reversible resistive switching, resistive random access memory (RRAM), conductive atomic force microscope

PACS: 72.20.–i, 68.35.bg, 71.30.+h, 73.40.Sx **DOI:** 10.1088/1674-1056/22/3/037201

1. Introduction

Switching memory (RRAM) utilizes an electric-field-induced resistive switching phenomenon and has attracted considerable attention as a candidate for the next generation of high-density nonvolatile memory, due to its low-voltage operation, high programming speed, and simple fabrication. Resistive switching in simple binary metal oxide thin films, such as SiOx,[1] TiO_2,[2,3] WOx,[4] ZnO,[5] ZrO_2,[6,7] and MgO[8] attracts great interest for possible applications in nonvolatile memory devices. Compared with more complex materials, such as $(Pr_{1-x}Ca_x)MnO_3$ or Cr-$SrZrO_3$, these simple binary oxide materials are more compatible with CMOS technology due to the simple fabrication process. Tran *et al.*[9] studied a unipolar RRAM based on a NiSi/HfOx/TiN structure, and observed a good memory performance in terms of on/off resistance ratio, retention, and readout margin. Chen *et al.*[10] reported the electrical characteristics of a room-temperature-fabricated Al/ZnO/Si memory device. They proposed that the resistive switching originates from the formation and dissolution of the AlOx barrier layer which are induced by the migration of the oxygen ions. Yu *et al.* [11] studied the characterization of low-frequency noise (LFN) in HfO_2-based RRAM. The LFN behavior was attributed to the distribution of the relaxation time of electron tunneling between the electrode and traps in the conductive filaments (CFs). Given that the RRAM can be embedded on a logic chip with the least amount of power consumption for programming and sufficiently long retention with a lower cost of manufacturing, more challengeable issues arise: which is the best material system of binary metal oxide films for RRAM application? Do we have enough fundamental understanding of the switching mechanism? How do set and reset the current affecting the circuits?

Vanadium oxide is also a traditional binary compound with different polymorphs. As we know, the ability of VO_x (such as VO_2, V_2O_3, and V_2O_5) to switch its conductance between two distinct states (insulator and metal) provides the basis for many electronic devices such as "smart windows" for energy saving and comfort, Mott field-effect transistors, electrical–optical switching devices, and thermal sensors.[12–16] The relaxation time to the coexistence state of vanadium dioxide is compatible with non-volatile memory requirements being longer than 10 years, that after 10 years the separation between the high and low resistance states would still be large enough for memory application[17] and the nanoscale vanadium oxide (VO_x) cell exhibited self-selective performance and memory switching by electroforming.[18] Vanadium oxide shows potential applications in the next generation nonvolatile memory field, more research efforts should be focused on the effect of the vanadium oxide on resistance switching (RS) properties.

*Project supported by the Program for New Century Excellent Talents in University of Ministry of Education of China (Grant No. NCET-11-1064), the Young Scientists Fund of the National Natural Science Foundation of China (Grant Nos. 61101055, 61274113, and 11204212), the Specialized Research Fund for the Doctoral Program of Higher Education of China (Grant No. 20100032120029), and Tianjin Natural Science Foundation of China (Grant No. 10SYSYJC27700).

†Corresponding author. E-mail: kailiang_zhang@163.com

© 2013 Chinese Physical Society and IOP Publishing Ltd

In this paper, mixed phase (V^{5+}, V^{4+}, and V^{3+}) VO_x-based memory devices with a Cu/VO_x/Cu structure were fabricated to study the resistive switching behaviors for RRAM applications. A unique reproducible nonpolar resistive switching behavior was observed in our VO_x system. The filament switching mechanism was investigated by using a conductive atomic force microscope (CAFM). The results are expected to provide the scientific basis for the design of vanadium-oxide-based memory devices.

2. Experimental procedure

A VO_x-based RRAM cell with a copper bottom electrode was fabricated. Before depositing the copper bottom electrode, a 5-nm-thick Ti layer for the adhesion layer was deposited on SiO_2/Si substrate by ion beam sputtering. After that, 200-nm Cu was deposited on the Ti layer as the bottom electrode by direct current sputtering. The flow ratio of Ar was 20 sccm, and the sputtering power was 30 W. The temperature and working pressure of the deposition process were 200 °C and 1.5 Pa, respectively.

The resistance switching layer, a 300-nm-thick VO_x thin film, was deposited on Cu/Ti/SiO_2/Si substrate by reactive sputtering with the vanadium target. The sputtering was carried out in Ar+O_2 mixed gas ambient, the flow ratio of Ar to O_2 was 4:1 with a total flow rate of 30 sccm, and the sputtering power was 200 W. The substrate temperature and working pressure of the deposition process were 350 °C and 1 Pa, respectively. The *I*–*V* characteristics were found using a two-probe technique with a copper micro-tip as the top contact for the VO_x film and the deposited copper as the bottom contact. Then, the Cu/VO_x/Cu memory cell was fabricated.

The surface micro-structure of the VO_x we deposited was investigated using an atomic force microscope (AFM). X-ray diffraction (XRD) and X-ray photoemission spectroscopy (XPS) analysis were used to identify the structure and composition of the grown VO_x film. All the electrical characteristics were tested by using a semiconductor device analyzer (B1500A). The relative micro-analysis of *I*–*V* characteristics of VO_x/Cu was characterized by the CAFM.

3. Results and discussion

Figure 1 shows the surface morphology of the VO_x film. The surface morphology of the VO_x exhibits fine granular crystallites. The crystalline structure of VO_x is determined by XRD, as shown in Fig. 2. The peaks at $2\theta = 21.4°$, $2\theta = 23.6°$, and $2\theta = 26.5°$ correspond to reflections in the (101), (201), and (211) planes of the V_2O_5 and VO_2 phase, respectively.

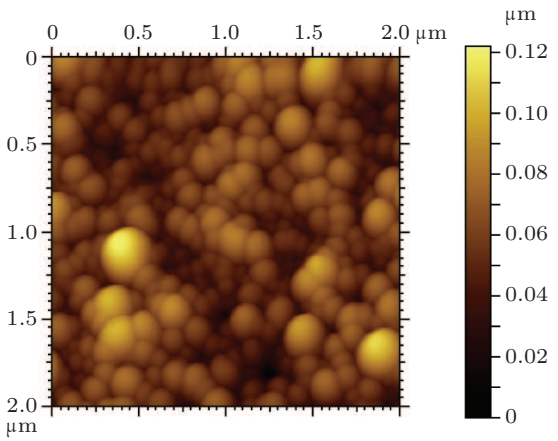


Fig. 1. (color online) AFM image of VO_x.

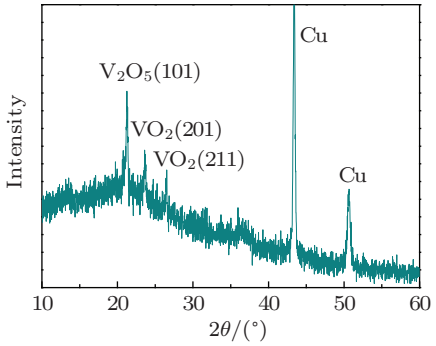


Fig. 2. (color online) Typical XRD diffraction spectra of VO_x.

In order to further define the components of the film, XPS was employed to examine the composition of the film. Figure 3(a) shows the XPS spectra of VO_x in the O1s, $V2p_{3/2}$, and $V2p_{1/2}$ regions, and $V2p_{3/2}$ peak appears at 517 eV. In Fig. 3(b), we compare the line shapes of the $V2p_{3/2}$ peaks of the VO_x. We identify three dominant components of the deconvolution labeled by V_3, V_4, and V_5. We attribute this structure to the significant presence of V^{3+} (515.99 eV), V^{4+} (516.88 eV), and V^{5+} (517.62 eV) peaks in the $V2p_{3/2}$ envelope. One test of our interpretation of the deconvolution is to compare estimated values of the average stoichiometry based on the ratios of these three components with values determined from the ratios of areas under the V and O peaks. The areas under the V^{3+}, V^{4+}, and V^{5+} peaks in the deconvolution of Fig. 3(b) provide the ratios of $\sim 17.96\%$ (V_2O_3), $\sim 37.56\%$ (VO_2), and $\sim 44.48\%$ (V_2O_5). From the above results, we can learn that the vanadium oxide deposited was in a mixture phase.

The typical formation process can be achieved under either positive or negative voltage, and the current compliance (CC, 5 mA) is used in the forming process in order to avoid irreversible memory cell damage. That is to say, dielectric breakdown takes place either with positive or negative sweep. After the forming operation, the cell is switched from a high resistance state (HRS: OFF state) to a low resistance state (LRS: ON state).

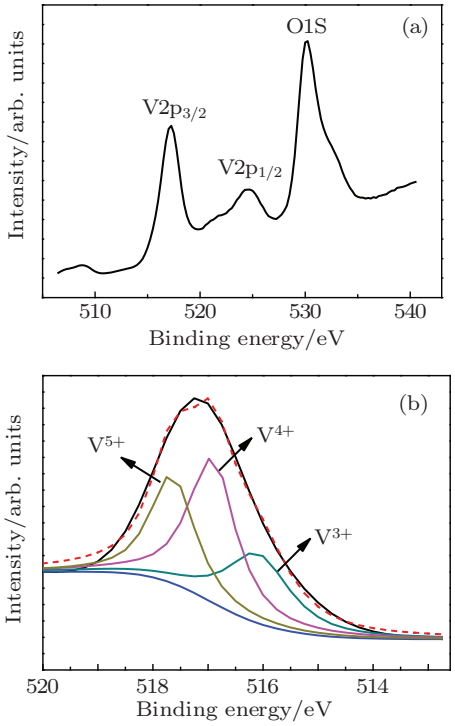


Fig. 3. (color online) (a) XPS spectra of VO_x. (b) Deconvolution of the $V2p_{3/2}$ peaks.

Figure 4 shows the typical reset (from LRS to HRS) and set operations (from HRS to LRS) under positive and negative voltage sweeps, respectively. The curves of a, b, c, and d depict positive reset, positive set, negative reset, and negative set process, respectively. Obviously, reversible resistive switching was realized in our VO_x system. Curve e shows the bipolar switching characteristic of the same device. When a positive bias was applied, the current level was abruptly increased, which is defined as the set state. Then, a bias was applied in reversed polarity, a relatively smooth current decrease was observed in the reset state, compared with the unipolar case. Therefore, both bipolar and unipolar reversible resistive switching are shown in this VO_x cell.

There are several possible ways to cause a high conduction path in a bipolar switching state. Severe off-stoichiometry, allowing a very conductive state, in a local region may be possible. The Joule heating may raise the local temperature around the filaments high enough to allow a stoichiometry change and even phase transformation.[19] In addition, it is known that oxygen desorption and adsorption can modify the local barrier height at the metal–oxide interface. Further investigations are expected to reveal the switching mechanism.

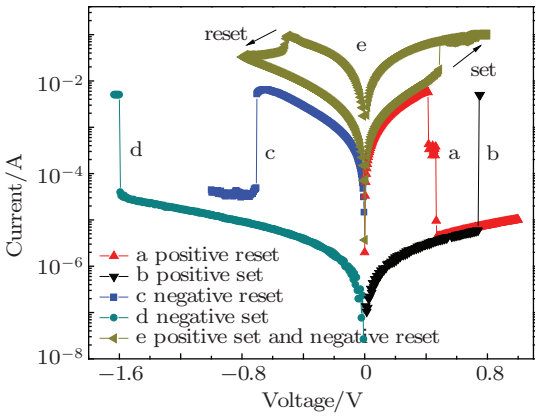


Fig. 4. (color online) *I–V* characteristics for Cu/VO_x/Cu cell under different voltage sweep directions.

The typical bipolar switching characteristics of a Cu/VO_x/Cu cell are presented in Fig. 5. Stable bipolar resistive switching behavior is observed (100 time cycles) and the programming voltage sweep was set to be −0.8, 0, 0.6, 0, −0.8 V, as shown by the arrows in Fig. 5(a). Figure 5(b) shows the distributions of set voltage and reset voltage of Cu/VO_x/Cu cell during 100 cycles. The average values of V_{set} and V_{reset} are 0.46 V and −0.49 V, respectively. Both the V_{set} and V_{reset} show narrow dispersions, indicating their excellent stability. The inset in Fig. 5(b) shows the double-logarithmic plots of the positive voltage sweep of the e curve in Fig. 4. Ohmic conduction characteristic with the slope of ∼ 1 is observed in the LRS, indicating the formation of conductive filaments during the set process. However, the conduction mechanism in the HRS is more complex. The slopes of the log*I*–log*V* of HRS change from 1 to 4.2. This behavior is in qualitative agreement with the trap-associated space-charge limited current (SCLC) theory.[5]

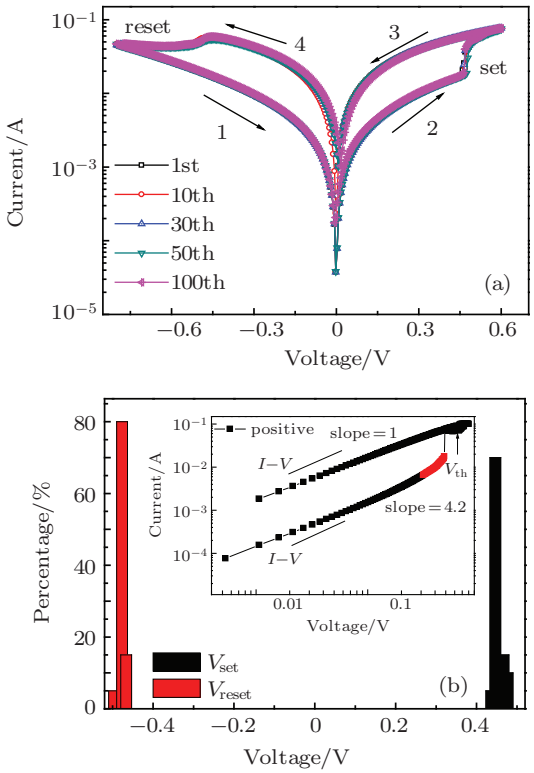


Fig. 5. (color online) Typical bipolar switching characteristics of Cu/VO_x/Cu cell. (a) *I–V* curves (100 cycles). (b) Distributions of V_{set} and V_{reset} in 100 cycles. The inset shows the *I–V* curves in log-log scale and the corresponding slopes for positive voltage sweep.

A schematic diagram of the CAFM process is shown in Fig. 6(a). The voltage was applied to the bottom electrode during the CAFM scan, and the bias polarity was defined as the tip bias polarity. Figures 6(b) and 6(c) show simultaneously acquired topographic and *in-situ* current images of the VO_x/Cu film with a sensing voltage of 0.1 V. First, the forming process was operated in a 5×5 μm^2 area, and the film was switched to a low resistance state. On the LRS (region A (forming), C (positive set), and E (negative set)), the multiple peaks in Fig. 6(c) indicate localized high conductance paths. The highly local electrical conduction was well resolved irrespective of the switching polarity. The peaks with high current must correspond to the locations where the filaments almost connect the tip and Cu back electrode. On the HRS (region B (positive reset) and D (negative reset)), the current peaks disappeared. The uniformly low current images were observed in the HRS region according to both bias polarities, respectively. Based on these results, the unipolar switching mechanism of VO_x system can be explained by filament mode.

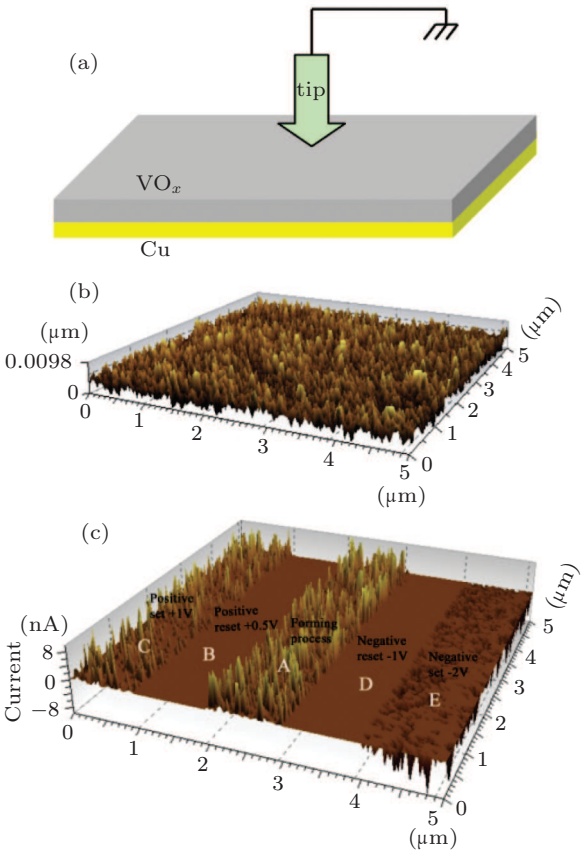


Fig. 6. (color online) (a) Schematic diagram of CAFM measurement setup. (b) Simultaneously obtained topographic image and (c) current image of VO_x thin films with a sensing voltage of 0.1 V of VO_x/Cu cell.

Figure 7 shows the set and reset voltage distribution for negative and positive sweep in 100 dc cycles. From Fig. 7, it can be seen that both the set and reset voltages for negative voltage sweep are larger than those for the positive voltage sweep. The discrepancy may be due to vanadium oxide sandwiched between an electrochemical working electrode (BE–Cu thin film) and an inert counter electrode (TE–Cu tip). Unipolar resistive switching with a Cu electrode is attributed to the migration of metal cations and the corresponding electrochemical metallization. The BE is more likely to undergo redox reaction than TE, so that both the set and reset voltages for negative voltage sweep are larger than the voltages for positive voltage sweep.

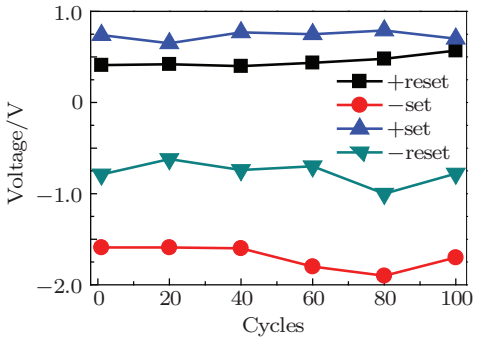


Fig. 7. (color online) Distribution of the set and reset voltages for negative and positive voltage sweep in 100 cycles.

Figure 8 shows the data retention for unipolar and bipolar at 120 °C. The results reveal that both unipolar and bipolar behaviors of the device can retain stable HRS and LRS without degradation for longer than 10^4 s, but the resistance value of the bipolar is much lower than that of the unipolar. This result was caused by different sweep modes for bipolar and unipolar RS. After the forming process, in the applied voltage range of 0–1 V or 0–2 V, the reset processes occurred. Conversely, the programming voltage sweep was in the order of −0.8, 0, 0.6, 0, and −0.8 V, the device was switched toward lower resistance state in positive voltage and then back into HRS in negative voltage. Namely, after forming process, the first set and then the reset processes occurred for bipolar RS. Thus, the resistance value of the bipolar is much lower than that of the unipolar.

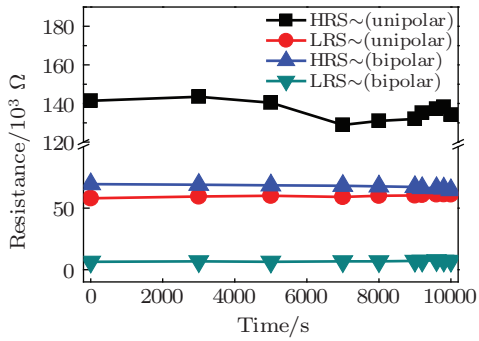


Fig. 8. (color online) Retention characteristics for both unipolar and bipolar at 120 °C.

4. Conclusion

We prepared mixture phase (V^{5+}, V^{4+}, and V^{3+}) VO_x film on a Cu/Ti/SiO_2/Si substrate by reactive sputtering. The

reversible resistive switching characteristics of a Cu/VO_x/Cu cell have been demonstrated. The *I*–*V* results indicate that unipolar and bipolar resistive switching behaviours coexist in our Cu/VO_x/Cu system. We directly observe the forming and removing of filaments at the HRS and LRS by CAFM measurements. The unipolar and bipolar switching mechanisms of VO_x system can be explained by filament mode and trap-associated SCLC theory, respectively. Important reliability investigations demonstrate the good endurance and retention behaviour of the Cu/VO_x/Cu cell. Reproducible switching behaviors and the simple fabrication process of the VO_x films are very attractive for nonvolatile memory applications.

References

[1] Wang Y Z, Chen Y T, Xue F, Zhou F, Chang Y F, Fowler B and Lee J C 2012 *Appl. Phys. Lett.* **100** 083502

[2] Meng Y, Zhang P J, Liu Z Y, Liao Z L, Pan X Y, Liang X J, Zhao H W and Chen D M 2010 *Chin. Phys. B* **19** 037304

[3] Wen X Z, Chen X, Wu N J and Ignatiev A 2011 *Chin. Phys. B* **20** 097703

[4] Li Y T, Long S B, Liu Q, Wang Q, Zhang M H, Lü H B, Shao L B, Wang Y, Zhang S, Zuo Q Y, Liu S and Liu M 2010 *Phys. Stat. Sol. (RRL)* **4** 124

[5] Wang H J, Zou C W, Zhou L, Tian C X, Lee M K and Lee J C 2011 *Phys. Stat. Sol. (RRL)* **5** 223

[6] Wu M C, Wu T H and Tseng T Y 2012 *J. Appl. Phys.* **111** 014505

[7] Guan W H, Long S B, Liu Q, Liu M and Wang W 2008 *IEEE Electron Dev. Lett.* **29** 434

[8] Huang H H, Shih W C and Lai C H 2010 *Appl. Phys. Lett.* **96** 193505

[9] Tran X A, Zhu W G, Gao B, Kang J F, Liu W J, Fang Z, Wang Z R, Yeo Y C, Nguyen B Y, Li M F and Yu H Y 2012 *IEEE Electron Dev. Lett.* **33** 4

[10] Chen C, Pan F, Wang Z S, Yang J and Zeng F 2012 *J. Appl. Phys.* **111** 013702

[11] Yu S M, Jeyasingh R, Wu Y and Wong P H S 2012 *Phys. Rev. B* **85** 045324

[12] Heckman E M, Gonzalez L P, Guh S, Barnes J O and Amelia C 2009 *Thin Solid Film.* **518** 1

[13] Liang J R, Hu M, Kan Q, Liang X Q, Wang X D, Li G K and Chen H D 2011 *Rare Metals* **30** 247

[14] Dejene F B and Ocaya R O 2010 *Curr. Appl. Phys.* **10** 508

[15] Kang M, Kim I, Kim S W, Ryu J W and Park H Y 2011 *Appl. Phys. Lett.* **98** 131907

[16] Liu X H, Zhang Y F, Yi S P, Huang C, Liao J, Li H B, Xiao D and Tao H Y 2011 *J. Supercritical Fluids* **56** 194

[17] Radu I P, Martens K, Mertens S, Adelmann C, Shi X, Tielens H, Schaekers M, Pourtois G, Elshocht S V, Gendt S D, Heyns M and Kittl J A 2011 *ECS Trans.* **35** 233

[18] Son M W, Liu X J, Sadaf S M, Lee D, Park S, Lee W, Kim S, Park J, Shin J, Jung S J, Ham M H and Hwang H 2012 *IEEE Electron Dev. Lett.* **33** 5

[19] Kim D C, Seo S, Ahn S E and Suh DS 2006 *Appl. Phys. Lett.* **88** 202102